Fire Induced Flow Field—Theory and Experiment

HOWARD R. BAUM
Center for Fire Research
National Bureau of Standards
Gaithersburg, Maryland 20899, USA

BERNARD J. MCCAFFREY
University of Maryland
College of Engineering
Baltimore, Maryland 21228, USA

ABSTRACT

The complete flow pattern induced by unconfined fires is studied theoretically and experimentally. The theoretical development is based on kinematic relationships between the velocity, vorticity, and heat release fields. The flow both inside and outside a single fire plume is related to plume centerline velocity and temperature measurements. Very large area fires, such as those hypothesized in the Nuclear Winter scenario, are represented as ensembles of individual fires of differing strengths distributed over randomly chosen sites within the burning area. The experimental data for fire plumes over a four order of magnitude size range is compared with these calculations and previously developed plume velocity and temperature correlations.

INTRODUCTION

The study of flows induced by isolated unconfined fires is of interest for two reasons. First, this represents the simplest configuration in which to study the structure of the fire plume and its effect on the environment, without the additional complexities introduced by enclosure geometries and ventilation systems. Second, large fires can often be considered to be composed of one or more such flow systems, so that it is useful to have a methodology capable of predicting their properties. While there is a considerable body of literature describing fire induced flows in enclosures (for an excellent survey see Zukoski (1)), there is much less information available describing the winds induced by unconfined fires.

An idealization usually made in the study of enclosure fires is that the fire plume pumps a stationary layer of cool gas through the heat release region into a nearly quiescent hot layer. The only motions of interest outside the plume are those induced by the presence of boundaries. However, the role of the plume as a fluid pump implies that this picture is incomplete. The fact that the plume gases entrain air as they rise means that a flow must be induced in the environment surrounding the fire. While the mean velocities associated with this flow are small compared with those in the plume for a single isolated fire, the composite mean horizontal velocity induced by a large number of such fires

can considerably exceed the plume vertical velocity. Carrier, et at. (2) have explicitly noted the need to account for such winds in their study of urban fire storms.

The first systematic calculation of the mean flow induced outside the fire plume was carried out by Taylor (3), who replaced the mass entrained into a point source plume by a line of sinks distributed along the plume centerline, and calculated the resulting potential flow. This calculation is the essential starting point for the approach to be followed here; yet it suffers from two basic limitations. First, even though the experimental data base available today is much better than that available to Taylor, so that it is not necessary to assume a point source plume, the direct measurement of entrainment which yields the sink strength is still a very difficult one. Second, the replacement of the fire plume by a line sink is not a good approximation near the edge of the plume itself. Moreover, this replacement furnishes very little guidance for the prediction of time dependent phenomena.

The basic difficulty can be traced to the fact that the velocity field, unlike the temperature field, does not have any sharp cutoff or change in character at the plume boundary. The flow quantity most like the temperature is in fact the vorticity, which can only be generated by solid boundaries and essentially horizontal temperature gradients in plumes. This is not inconsistent with Taylor's picture, and lends itself to a "kinematic" approach to fire induced flows. This kinematic approach, set out in the next two sections below, regards the vorticity and rate of heat release as the fundamental sources of the flow, both inside and outside the fire plume. This method of analysis can be applied to either time dependent or time averaged descriptions of the flow. The main requirement is the existence of a plume data base from which the vorticity field can be inferred.

The data needed for the time averaged plume vorticity distribution is obtained from McCaffrey's (4) plume correlation. This correlation was assembled from an analysis of small scale laboratory plume centerline velocity and temperature measurements. Since that time many larger scale experiments have been performed, permitting the validity of this correlation to be assessed over a range of four orders of magnitude in fire strength. Time resolved data has also begun to appear. The status of the relevant experimental data base is discussed in the fourth section.

The "Nuclear Winter" hypothesis (5) has revived interest in the flows induced by very large fires. Here, the primary feature of interest is the fire induced convection column covering many kilometers in the horizontal directions and extending to the height of the atmosphere. Existing analyses of this phenomenon, whether analytical in nature (2), (6) or based on detailed time dependent numerical simulations (7)-(9), have represented the fires themselves as a smooth continuous source of heat. It is the present authors contention that a more realistic idealization for these or any other large fires is a random distribution of distinct fires with the same characteristics they would possess if isolated. This is certainly true if the fires are all widely separated from each other. While this is not necessarily always the case in a large urban fire, the analysis in the fifth section shows that global rates of heat release postulated in many of the simulations mentioned above can be readily achieved with distinct fires occupying only a small fraction of the nominally burning area.

This analysis is primarily aimed at describing the low level flows in the first few hundred meters above the firebed, before the individual plumes above each separate fire can merge. Even with this restriction, the calculation presents some severe computational problems. Even the time averaged velocity field involves a three order of magnitude range of length scales in the horizontal directions, and is inherently three dimensional. This fact, together with the random locations and varying strengths of the large number (hundreds to thousands) of fires used in the simulations, requires the development of some novel means of performing the calculations. Perhaps the most interesting result to emerge is the prediction of very large ground level horizontal inflows, without the need to invoke an external swirling velocity field far from the burning area.

The Kinematic Model

The flow induced by a large fire is primarily determined by three factors: The geometrical arrangement of the burning parcels of fuel, the rate of heat released by each individual fuel element, and the atmospheric environment in the neighborhood of the firebed. In any given fire scenario, there is a considerable amount of randomness in each of these factors. The mathematical model described below attempts to deal with this situation by combining random distributions of location and burning rate of the individual fuel elements with a deterministic description of the composite flow generated by a given realization of the fire scenario. Each fuel element is assumed to be sufficiently removed from the others so that the buoyant plume of hot gas and smoke rising above the burning fuel evolves independently. This assumption implies that attention is restricted to low altitudes, before the separate plumes merge into a large convective column. Thus, the atmospheric environment (winds and stratification) does not play a significant role in what follows. Under these circumstances, the composite flow field can be decomposed into a collection of individual flows associated with each plume. The flow pattern associated with a single plume can then be analyzed in detail and the results compared with experimental data.

The starting point is the inviscid equations of fluid mechanics which control the large scale fluid motion of interest. These laws expressing conservation of mass, momentum, energy, and an equation of state, for a low Mach number variable density flow are (10).

$$\begin{aligned} &\frac{D\rho}{Dt} + \rho\nabla\cdot\vec{u} = 0 \\ &\rho\frac{D\vec{u}}{Dt} + \nabla\tilde{p} - (\rho - \rho_o)\vec{g} = 0 \\ &\rho C_p \frac{DT}{Dt} = Q(\vec{r},t) \\ &P_o = \rho RT \end{aligned} \qquad (1)$$

Here ρ, $\vec{u}$, and T are, the local density, velocity, and temperature in the gas at position $\vec{r}$ and time t induced by a rate of energy release $Q(\vec{r},t)$. The gas has a specific heat C_p and gas constant R, while $\vec{g}$ is the gravitational acceleration. The quantities P_o and ρ_o are ground level ambient pressure and density, while $\tilde{p}$ represents the small perturbation from hydrostatic pressure that drives the motion. All plumes are assumed to evolve in a uniform atmosphere at rest far from the plumes. The convective operator D/Dt includes local time dependence:

$$\frac{D}{Dt} \equiv \frac{\partial}{\partial t} + \vec{u}\cdot\nabla$$

It is certainly not feasible to contemplate solving eq. (1) directly. Instead, we make use of two equivalent results. If the first of eqs. (1) is multiplied by C_p and added to the third and the equation of state is used, the divergence of the velocity field can be expressed as:

$$\nabla\cdot\vec{u} = Q(\vec{r},t)/\rho_o C_p T_o \tag{2}$$

Physically, eq. (2) states that the volumetric expansion rate of any fluid element is proportional to the net rate of heat addition. It is important to note that although the heat is added to the atmosphere only in the vicinity of each element of burning fuel, eq. (2) is valid everywhere above the surface. The second result needed is Bjerknes theorem (11). The fluid vorticity $\vec{\omega}$ is defined in terms of the fluid velocity $\vec{u}$ as:

$$\nabla\times\vec{u} \equiv \vec{\omega} \tag{3}$$

Now consider a closed loop of Lagrangian marked particles moving with the local fluid velocity. The circulation Γ around that closed loop is defined as:

$$\Gamma \equiv \oint_{\ell}\vec{u}\cdot d\vec{r} = \oint\vec{\omega}\cdot\vec{n}dA \tag{4}$$

Here $\vec{n}$ is a unit vector normal to any surface A bounded by the closed loop ℓ of marked particles. The momentum conservation equation, the second of eq. (1), can then be manipulated into the form:

$$\frac{d\Gamma}{dt} = \oint_{\ell}\{[(\rho - \rho_o)/\rho_o]\vec{g} - \nabla\tilde{p}/\rho\}\cdot d\vec{r} \tag{5}$$

Equation (5) is Bjerknes theorem. Physically, it states that vorticity can be created in a fluid away from a boundary only through the mechanism of density gradients. In the absence of such gradients the circulation around the closed loop, and hence the vorticity contained within the loop, cannot change.

Now consider the history of a fluid element originating from rest far from any of the plumes generated by the fire. Initially the fluid contained no vorticity, and in its approach to the fire it remains irrotational. As it enters one of the plumes it encounters large density gradients, and an intense vortex field is created. Thus, eq. (3) can be rewritten as:

$$\nabla\times\vec{u} = \vec{\omega}_p(\vec{r},t) \tag{6}$$

Here $\vec{\omega}_p$ denotes the vorticity in the plumes. Just as in the case of eq. (2), eq. (6) holds everywhere even though $\vec{\omega}_p$ only involves the velocity gradients inside the plumes.

Two further points should be noted. First, since the right hand sides of eqs. (2) and (6) involve only information inside the plumes, if the plumes remain distinct we can write:

$$Q(\vec{r},t) = \sum_i Q_i(\vec{r},t) \qquad \vec{\omega}_p(\vec{r},t) = \sum_i \vec{\omega}_{pi}(\vec{r},t) \tag{7}$$

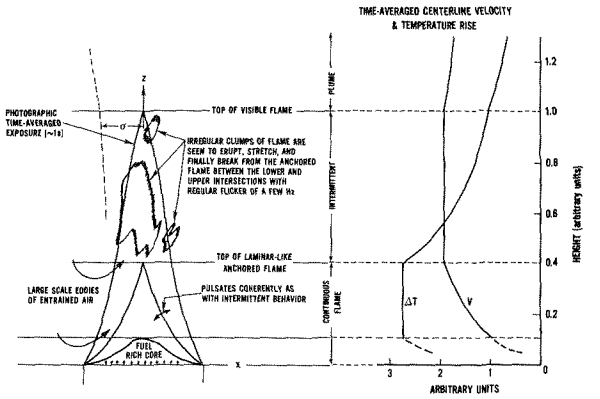

Figure 1. Conceptual picture of buoyant diffusion flame.

Here the sum is taken over each individual plume. Thus, a velocity field $\vec{u}_i$ can be associated with each plume, where the velocity field is the solution to

$$\nabla \cdot \vec{u}_i = Q_i / \rho_o C_p T_o \qquad \nabla \times \vec{u}_i = \vec{\omega}_{pi} \tag{8}$$

Second, these formulae are valid both instantaneously and in a time averaged sense. If time dependent information about the structure of an individual fire plume is available, then it can be used in eq. (8). At present, only time averaged information is available. In either case, the kinematics of a general vector field insures that a knowledge of the divergence and curl of the vector is sufficient to determine it everywhere uniquely.

The next step in the analysis is the representation of the vorticity and rate of heat release fields, the right hand side of eqs. (8). There is ample experimental support (4) for a Gaussian radial distribution for the time averaged vertical velocity u and temperature rise $T-T_o$ in the central region of a buoyant plume. Thus, these quantities can be represented in the form

$$u = U(z) \exp\left\{-[r/R(z)]^2\right\}$$
$$(T-T_0)/T_0 = \Theta(z)\exp\left\{-[r/\lambda R(z)]^2\right\} \tag{9}$$

Here, z denotes vertical distance above ground level and r radial distance from the mean plume centerline. The quantity λ represents the ratio of thermal to velocity plume widths. The time averaged convective energy flux in the plume at any height, H(Z), is given by:

$$H(z) = 2\pi C_p \int_0^\infty \rho u (T-T_0) r dr \tag{10}$$

Since H(z) is closely related to the heat release distribution, a quantity presumed known in this study, three more pieces of information are required to completely specify the profiles given in eqs. (9). In principle, one could proceed by adopting an integral approach, using the

conservation of mass and vertical momentum averaged over the plume cross section together with an estimate of λ to obtain the necessary information. However, that immediately leads to a requirement to estimate the entrainment rate and the difficulties noted above. The alternative approach adopted here is to employ the correlations developed in Ref. (4) to estimate U, Θ, and λ directly.

Before examining the correlations and their consequences, it is important to get a better idea of the plume structure. Fig. (1) shows an idealization of a typical pool fire or low momentum burner flame. There are three reasonably distinct regions. The lowest region is the continuous burning zone. There are always many flame sheets anchored to the fuel bed. The flow is not steady, but pulsates fairly regularly as large scale eddies are entrained into the plume. The second region is an intermittent zone containing irregular patches of flame breaking off from the anchored flame. At the top of the visible flame zone, almost all combustion has ceased. Above this point is the plume region, characterized by the classical velocity and thermal structure induced by a weakly buoyant source. The forms chosen are not arbitrary, but make maximum use of the classical plume theory. The vertical distance, velocity, and temperature are made dimensionless as follows:

$$z(Q_o/\rho_o C_p T_o \sqrt{g})^{-2/5} \equiv z^* = z/D^* \tag{11}$$

$$U/\sqrt{gD^*} \equiv U^*(z^*) \tag{12}$$

$$\Theta \equiv \Theta^*(z^*) \tag{13}$$

In these equations, it is important to note that Q_o refers to the total chemical rate of heat release. A crude accounting for radiative losses will be made explicitly below.

The temperature and velocity correlations provide that U^* and Θ^* are the following functions of z^* only:

$$U^* = A(z^*)^n \qquad \Theta^* = B(z^*)^{2n-1} \tag{14}$$

TABLE 1. Plume Correlation Parameters

Plume	Range	n	A	B
Flame	$0<z^*<1.32$	1/2	2.18	2.91
Intermittent	$1.32<z^*<3.30$	0	2.45	3.81
Plume	$3.30<z^*$	-1/3	3.64	8.41

The quantities n,A, and B for each region are given in Table 1. The functions are sketched at the right of figure 1.

Substitution of eqs. (9) into eq. (10) then yields the following form for H(z).

$$H(z) = \pi C_p \rho_o T_o R^2 U(z)[1-I_\lambda(\Theta^*)] \tag{15}$$

$$I_\lambda(\Theta^*) = \int_0^1 dt \, \{1 + \Theta^*(t)^{1/\lambda^2}\}^{-1}$$

McCaffrey finds that $\lambda = 0.862$ everywhere in the plume represents the best fit to the data. This value is somewhat awkward to work with, since the integral I_λ must then be evaluated numerically. Examination of the data base used shows that a value $\lambda = \sqrt{3/2} = .866$ lies well within the scatter. With this choice of λ, the integral I can be evaluated in closed form as:

$$I_\lambda(a) = 3(\sqrt{2}a)^{-3/4} \{\log K + \pi - \arctan L - \arctan M\} \qquad (a) > (2)^{-1/2}$$

$$I_\lambda(a) = 3(\sqrt{2}a)^{-3/4} \{\log K + \arctan(-L) - \arctan M\} \qquad 0 \leq a \leq (2)^{-1/2}$$

$$K = \left\{ \frac{[(a)^{1/4} - (2)^{-1/2}]^2 + 1/2}{[(a)^{1/4} + (2)^{-1/2}]^2 + 1/2} \right\}^{1/2} \qquad (16)$$

$$L = (2)^{-1/2}[(a)^{1/4} - (2)^{-1/2}]^{-1}$$
$$M = (2)^{-1/2}[(a)^{1/4} + (2)^{-1/2}]^{-1}$$

Eqs. (14)-(16) can now be used to determine complete structure of the fire plume. At the top of the intermittent flame zone, the combustion has ceased. Thus, in the plume region, the convective energy flux H(z) must be constant and equal to the total chemical heat release Q_o minus the fraction radiated away. Denoting this fraction by η the plume radius can be readily obtained as:

$$R/D^* \equiv R^* = \{(1-\eta)/\pi U^*[1 - I_\lambda(\theta^*)]\}^{1/2} \qquad (17)$$

In the intermittent flame zone itself, there is still some combustion occurring, leading to an increase in H(z). However, this is roughly balanced by a small amount of radiation from the burning eddies. The net result is that the overall change in H(z) is very small and eq. (17) may be used all the way down to the end of the continuous flame zone with little loss in accuracy. Inside the continuous flame zone, energy is not conserved and H(z) changes rapidly. However, by analyzing the momentum equation, McCaffrey is able to show that the plume radius R^* is approximately constant. This statement does not hold immediately adjacent to the burner or fuel bed, where the whole idea of a plume as a slender object breaks down. However in the upper half of the continuous flame zone, eq. (17) can be replaced by:

$$R^* = R^*_f \equiv R^*(z^* = 1.32) \qquad (18)$$

The radiative fraction for fires using relatively smoke free hydrocarbon fuels is generally in the range 0.25 - 0.35. It can change dramatically, however, for large fires with heavy smoke loading. This is one reason for wanting to display the radiation loss explicitly. It is also true that in many fire experiments it is impossible to determine the rate of heat release directly. The quantity actually measured is the weight loss of the burning object as a function of time. This information, together with tests on small scale samples to yield heat release rate per unit mass leads to an inferred value of the chemical heat release rate rather than the convective energy flux. Hence, an explicitly correction is required.

With U and R determined, the vorticity $\vec{\omega}$ is then given by:

$$\vec{\omega} = \omega_\phi \vec{\phi} \tag{19}$$
$$\omega_\phi = [2U(z)/R(z)]\left\{(r/R)\ \exp\ [-(r/R)^2]\right\}$$

Here $\vec{\phi}$ is a unit vector in the azimuthal direction. The time averaged vorticity is seen to be distributed in azimuthal rings about the axis of symmetry of the plume. The time averaged rate of heat release Q is related to the function H(z) by:

$$\frac{dH}{dz}(z) = 2\pi\int_0^\infty drrQ(r,z)(1-\eta) \tag{20}$$

Equation (20) together with the additional assumption of a Gaussian profile whose width is given by eq. (18) then uniquely determines Q.

The Single Plume Flow Field

The problem of solving for the mean induced velocity field now reduces to the solution of eqs. (2) and (6) for the prescribed values of Q and $\vec{\omega}$. The result is actually a kinematically and (approximately) dynamically consistent flow field both inside and outside the plume. The calculation is performed by decomposing the velocity field into solenoidal and irrotational components.

$$\vec{u} = \nabla\Phi + \vec{v} \qquad \nabla \cdot \vec{v} = 0 \tag{21}$$

Since the time averaged vorticity and heat release distributions are axially symmetric, the vertical and radial velocity components u_z and u_r can be obtained in terms of $\Phi(r,z)$ and a pseudo-stream function $\Psi(r,z)$ as follows:

$$u_z = \frac{\partial\Phi}{\partial z} + \frac{1}{r}\frac{\partial\Psi}{\partial r} \qquad u_r = \frac{\partial\Phi}{\partial r} - \frac{1}{r}\frac{\partial\Psi}{\partial z} \tag{22}$$

The equations are made non-dimensional by introducing the velocity and length scales defined in equations (11) and (12). The rate of heat release is normalized as follows:

$$Q(r,z) = [Q_o/(D^*)^3]\tilde{Q}(r^*,z^*) \tag{23}$$

The remaining variables are scaled in the form:

$$(u_r,\ u_z) = (gD^*)^{1/2}\left\{\tilde{u}(r^*,z^*),\ \tilde{v}(r^*,z^*)\right\}$$
$$(\Phi,\Psi) = (gD^*)^{1/2}D^*\left\{\tilde{\Phi}(r^*,z^*),\ \tilde{\Psi}(r^*,z^*)\right\} \tag{24}$$
$$\omega_\phi = (g/D^*)^{1/2}\tilde{\omega}(r^*,z^*); \qquad r = D^*r^*; \qquad z = D^*z^*$$

Now dropping all tildes and asterisks, the equations for Φ and Ψ become:

$$\frac{1}{r}\frac{\partial}{\partial r}\left(r\frac{\partial\Phi}{\partial r}\right) + \frac{\partial^2\Phi}{\partial z^2} = Q(r,z)\ ;\ \frac{\partial^2\Psi}{\partial z^2} + \frac{\partial^2\Psi}{\partial r^2} - \frac{1}{r}\frac{\partial\Psi}{\partial r} = r\omega(r,z) \tag{25}$$

Equations (25) must be solved subject to the boundary condition u = 0 at the surface z = 0. The additional no-slip boundary condition, v = o, cannot be enforced in an inviscid model. Far from the heat source in every direction u and v vanish at least as fast as $(r^2 + z^2)^{-1/3}$, since

that is the asymptotic decay rate in the plume. In addition, the spatial extent of the heat source is bounded. Hence, the potential flow at infinity must be equivalent to that from a point source. Mathematically, these conditions can be expressed in the form:

$$\Psi(r,0) = \frac{\partial \tilde{\Phi}}{\partial z}(r,0) = 0 \qquad (26)$$
$$\lim_{r,z \to \infty} (\Phi,\Psi) = 0$$

Solutions to equations (25) are obtained numerically using finite difference methods using the FISHPAK (12) separable elliptic equations solvers. These (or indeed any) algorithms can only give accurate results when employed on a finite domain. The solutions obtained must retain their accuracy in the infinite domain, however, if they are to be useful in large area fire simulations. This can be accomplished by replacing boundary conditions at infinity by analytical asymptotic solutions to eqs. (25) and (26). The asymptotic solutions are then assumed to apply outside a large but finite cylindrical domain. The numerical solutions are employed inside this domain, with the asymptotic results used as boundary conditions.

The asymptotic solution corresponding to the potential induced by a point source is:

$$\Phi = (1-\eta)/2\pi(r^2+z^2)^{1/2} \qquad (27)$$

Physically, the volumetric source representing the non-radiating fraction of the heat released pushes all the fluid into the upper half plane along straight streamlines originating from the source.

Next consider the solenoidal flow pattern. This is much more interesting, due to the nature of the flow and because it dominates the motion far from the fire. The asymptotic form of ω is very simple when expressed in terms of a spherical radial coordinate ρ and polar angle θ.

$$\tilde{\omega} = (\rho)^{-4/3}\ \Omega(\theta) \equiv \omega_a$$

$$\Omega(\theta) = 2A\left[\frac{3\pi AB}{7(1-\eta)}\right]\tan\theta\ (\cos\theta)^{-4/3}\ \exp\left\{-\frac{3}{7}\frac{\pi AB}{(1-\eta)}\tan^2\theta\right\} \qquad (28)$$
$$\rho^2 = r^2 + z^2\ ;\ z = \rho\cos\theta\ ;\ r = \rho\sin\theta$$

The solution to the second of eqs. (25) with ω replaced by ω_a is obtained by assuming Ψ to have the form:

$$\Psi = (\rho)^{5/3}F(\theta) \qquad (29)$$

Then, using the variable $\mu = \cos\theta$ in eqs. (25), (28) and (29); the equation and boundary conditions for $F(\mu)$ are:

$$\frac{d^2F}{d\mu^2} + [10/9(1-\mu^2)]\ F = \Omega(\mu)$$

$$\Omega(\mu) = -\ 6\pi A^2B/[7(1-\eta)](\mu)^{-7/3}\exp\left\{-3\pi AB(1-\mu^2)/7\mu^2(1-\eta)\right\} \qquad (30)$$

$$F(0) = F(1) = 0$$

Note that the solution to eqs. (30) together with eq. (29) constitutes an exact solution of the second of eqs. (25) and the boundary conditions. The solution is obtained as follows:

Introduce a new variable x defined by:

$$x = (1 + \mu)/2 \; ; \qquad 1/2 \le x \le 1 \tag{31}$$

The homogeneous terms in eq. (30) then become:

$$x(1 - x)\frac{d^2F}{dx^2} + (\frac{5}{3})(\frac{2}{3})F = 0 \tag{32}$$

This is the hypergeometric equation. Let one solution to this equation which is bounded over the domain of interest be denoted $U_1(x)$. Then (13):

$$U_1(x) = x\ {}_2F_1\ (-\frac{2}{3},\ \frac{5}{3},\ 2, x)$$
$$ {}_2F_1\ (-\frac{2}{3},\ \frac{5}{3}, 2, x) = [\gamma(\frac{5}{3})\gamma(\frac{1}{3})]^{-1}\int_0^1 dt\{(1-xt)/(1-t)\}^{2/3} \tag{33}$$

Here γ denotes the Factorial function.

A second independent solution to the homogeneous equation $U_2(x)$ can readily be found in the form:

$$U_2(x) = U_1(x)\ v(x) \; ; \; v(x) = \int_x^1 dt\ [U_1(t)]^{-2} \tag{34}$$

The solutions U_1 and U_2 can be used to construct two other independent solutions W_1 and W_2, such that W_1 vanishes at $x = 1/2$ and W_2 vanishes at $x = 1$.

Denoting $\hat{U}_1(x)$ and $\hat{U}_2(x)$ the solutions given in eqs. (33) and (34) with the factor $\{\gamma^2(5/3)\ \gamma(1/3)\}^{-1}$ removed, the required solutions are:

$$W_1 = \hat{U}_1(x)\ \hat{U}_2(\tfrac{1}{2}) - \hat{U}_2(x)\ \hat{U}_1(\tfrac{1}{2}) \; ; \; W_2 = \hat{U}_2(x) \tag{35}$$

From these two solutions, it is a straightforward task to determine the solution to eq. (30) in the form:

$$F(x) = [\hat{U}_2(\tfrac{1}{2})]^{-1}\ \{W_2(x)\int_{1/2}^{x}\Omega(x_o)W_1(x_o)dx_o + W_1(x)\int_x^1 \Omega(x_o)W_2(x_o)dx_o\} \tag{36}$$

The solution given in eq. (36) is equivalent to that obtained by Taylor (3) outside the plume. However, unlike Taylor's result, eq. (36) is uniformly valid, with the plume flow incorporated in a kinematically consistent manner. (It is also dynamically consistent subject to the inherent limitations on our ability to predict turbulent flows). Figure (2) shows the angular dependence of the spherical polar radial (V_ρ) and angular (V_θ) components of the velocity field as determined from eqs. (29) and (36). The $(\rho)^{-1/3}$ radial dependence is suppressed in the figure by evaluating the velocities at $\rho = 1$. The radial velocity exhibits a strong outflow with a Gaussian profile in the plume centered at $\theta = 0$. This is exactly compensated by a weak inflow at all other angles down to the ground at $\theta = \pi/2$. The angular velocity is always small with no significant structure, vanishing at $\theta = 0$ and $\theta = \pi/2$. The radiative fraction is taken to be $\eta = 0.35$ in all calculations.

The asymptotic formulae were used as boundary conditions at the edge of a right cylinder of radius $r = 10$ and height $z = 20$. Since eqs. (29) and (36) are themselves exact solutions to the point source plume equations, they were employed as a test of the accuracy of the FISHPAK software for this problem. It was found that a discretization $\Delta r = \Delta z = 0.1$ was sufficient to guarantee a numerical error in the solutions of eq. (25) of less than 1/2 percent. Figure (3) shows a comparison of the

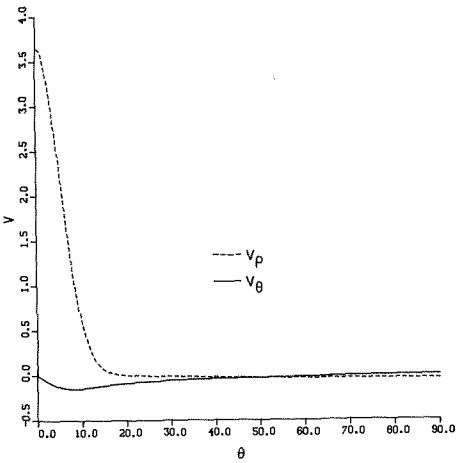

Figure 2. Angular dependence of radial V_ρ andtangential (V_θ) components of velocity for point source plume in spherical polar coordinates.

centerline vertical velocity computed by this method with that given by the correlation. It is a test of the internal consistency of the calculation. The lower solid line is the correlation characterized by table 1, with the upper solid line obtained from the numerical solutions to eqs. (22) and (25). The worst error is less than four percent. It is also clear that most of the flow is induced by the vortex field except

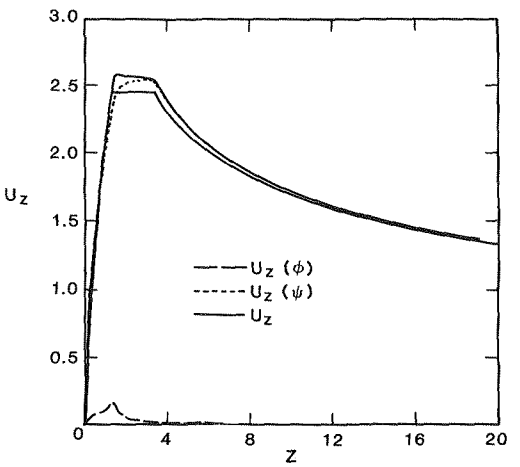

Figure 3. Comparison of computed centerline velocities (upper solid curve) with plume velocity correlation (lower solid curve).

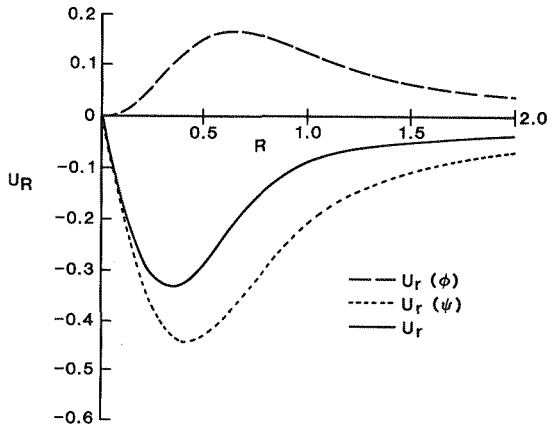

Figure 4. Calculated ground level radial velocity showing potential (dashed) and solenoidal (dotted) contributions to flow.

very close to the flaming region. This is also borne out by the ground level radial flow, plotted in Fig. (4). The vorticity induces a strong inflow which peaks near the edge of the plume, which is partially countered by the expansion induced by the local heat release. This effort rapidly diminishes with increasing r; so that by r = 10 the vorticity induced flow is overwhelmingly dominant.

The Experimental Database

The mathematical model developed above has been shown to be in reasonable agreement with correlations developed from small scale experiments. We now wish to compare the correlations with the experimental database.

Most of our knowledge of fire plumes, defined here as buoyant diffusion flames from area sources, comes from observations at laboratory scale, dimensions on the order of 1m. A variety of transducers including thermocouples, ionization probes, and bidirectional velocity probes have been inserted directly into these flames and recently several non intrusive optical devices including LDV's have been used for garnering further information. What has emerged is a qualitativae or descriptive picture of the phenomena illustrated in Fig. 1, and a quantitative description of the time-averaged behavior manifested in the correlations summarized in Table 1.

Diameter or heat release rate together with fuel type ought to completely define the problem, at least for a radiatively non-participating, quiescent, normal oxygen containing environment, i.e. D and Q are uniquely related for a given fuel type. Hasemi (14), Heskestad (15), and Cetegen et.al. (16) have all added refinements to the above interpretation in introducing to the temperature data analysis a virtual source, i.e., the place where one starts measuring z, which is a weak function of Q*. For simplicity we have ignored these variations since

further refinements (Hasemi (14) Appendix) may be required and also it may turn out that the effects are second order for large pool fires. In addition, more recent measurements [Rockett, Sugawa, McCaffrey (17)] indicate that the use of a virtual source actually makes the collapse of velocity data worse than if one were not used.

How well the small scale-developed analysis represents the behavior of fires can be estimated from Fig. 5. Time-averaged and scaled width, centerline velocity, and centerline temperature rise are shown plotted against scaled height. The lines represent the analytical predictions, the symbols are available literature data for pool diameters between 2 and 30 m. Two meters is an arbitrary compromise between having too many points from small fires and yet having a sufficient number of points, especially higher in the flame plume. Recall that fire size or, implicitly D, is contained in he denominator of scaled height.

In general the agreement between width and velocity data and the corresponding analysis seems reasonable. Recall that a Gaussian form was chosen for the radial variation. For the width plot the line is actually the 1/e profile for velocity while the three 15 m JP-4 points are 1/e temperature data. Measurements made at small scale indicated that the temperature rise profile was slightly narrower than the velocity profile. That difference is ignored here and the velocity profile will be used as the measure of plume width. (For the 15 m pool, data below 5.7 m exhibited a bimodel radial distribution and were, consequently not used for the present comparison since the analysis is no longer appropriate very near the surface.) Surprisingly, perhaps, the velocity data appear to scatter less and be in closer agreement with the analysis than does the temperature data. With the temperature data there appears to be a tendency for the temperature rise to increase with fire size for the larger fires. One can speculate that this may be the result of a thickening and slower moving soot layer surrounding the luminous portion of the flame plume which might tend to block the radiation from escaping.

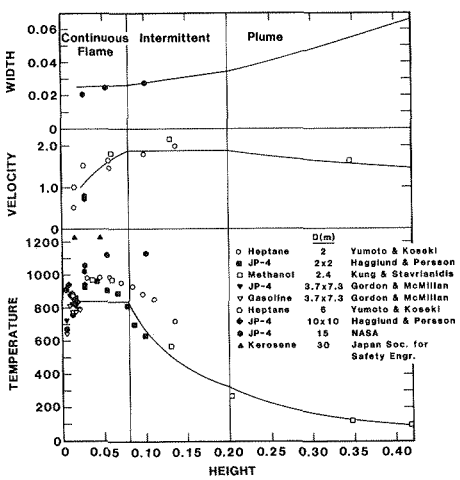

Figure 5. Comparison of large scale data with small scale correlation and analysis. For data sources see Refs. (28),(18),(31),(29),(32),(33).

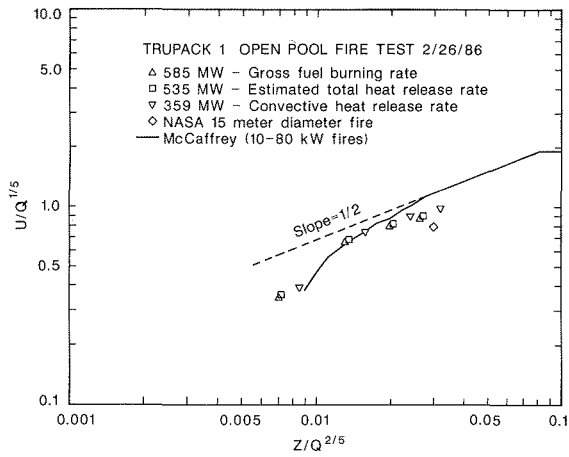

Figure 6. Comparison of fire hundred megawatt pool fire velocity measurements with correlation.

Decreasing radiant intensity with fire size due to soot blocking has been observed for increasing D (Hagglund and Persson (18) and for increasing Q (McCaffrey (19). The increased temperature levels on the centerline seen on Fig. 5 may be another manifestation of the same phenomenon.

Some very recent data has emerged for velocity in large pools of jet fuel used to evaluate the integrity of containment of nuclear waste material. Fig. (6) from Keltner, (20), shows the results of upward gas velocity measurements in the lower regions of the flames in comparison to the simple correlations presented earlier. Seen on the figure is a dashed line of slope 1/2, the approximately value of the slope in the continuous flame region, that is, up to about 0.08 in the units of the figure. The solid line is a representation of the actual data near the burner surface in the small scale result which is ignored in deriving the simple, 1/2 slope correlation. That is, the further away from the surface one travels the closer the data approaches the 1/2 slope. If it turns out that this starting region with time-averaged bimodal temperature distributions is important in characterizing the phenomena than Fig. 4 is a testament to the facet that the small scale measurements could in fact be used even to capture this behavior. The laboratory scale solid line appears to represent the one-half gigawatt data very adequately. Thus, the correlation is valid over a four order of magnitude range in Q.

We now turn to a discussion of time resolved data. Figure 7 showing the characteristic pulsation frequency plotted against fire size, D, attempts to further bridge small and large scale. Shown by open triangles is the data of Byram and Nelson (30)(1970) obtained by counting the "roaring sounds that accompanied the pulsations" of ethanol pool fires in a given interval of time. (For the smaller diameter fires high speed movie film was used). The value of approximately 3 Hz found earlier (21), (22) in 0.30 m square methane gas burner would fall within this data scatter. The filled symbols represent the large diameter Japanese crude oil and kerosene data. The solid line has a slope of -1/2 and represents a relatively smooth transition from small to large scale. The D to the -1/2 power follows directly from an inviscid-hydrostatic

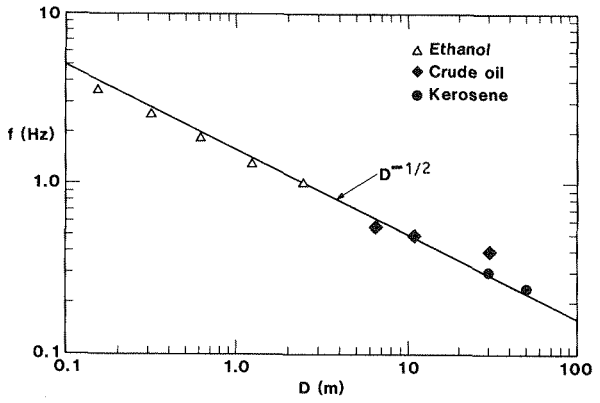

Figure 7. Pool fire pulsation frequency as function of diameter.

analysis with the inverse period being proportional to velocity divided by distance. Velocity is proportional to square root of diameter and dividing by distance which is proportional to D yields the requisite result. A smooth transition in the data does not guarantee the absence of any new phenomena associated with large fires. It is certainly, however, a necessary condition for such an absence. For example, in decreasing size, laminar-like diffusion flames of $D < 0.1$ m exhibit frequencies which would not be correlated by the line shown, i.e., $f\sqrt{D}$ becomes a function of D. In this case therefore possible new phenomena would be indicated.

To date most of our information comes from time-averaged measurements. The fire plume however, involves many different time scales ranging from submicrosecond molecular processes involving chemical changes through millisecond diffusional transport processes all the way up to seconds where large scale coherent eddy structures encompass the fluid mechanical mixing aspects. It is quite clear that time-averaging can only give a crude picture and will not provide the detailed information necessary for accurate analytical characterization. The next phase in this development is to assume the chemistry is infinitely fast and to try and resolve the slowest (which for these pool configured diffusion flames may be the most important) namely, to resolve the large scale mixing process. Non-stationary studies of the structure of the flow are taking place at several institutions including Waterloo (Wechman, et at (23)), Borehamwood/Southampton (Walker & Moss (24)), Washington State (Fisher, et al (25)) and Stuttgart (Schonbucher et al (26)). The analytical approach needed to provide a rational framework for this data has yet to be developed.

Large Fires

We now turn to the flows induced by fires spread over large urban or industrial areas. Such mass fires, whether induced by industrial accidents, earthquake, or war, could extend over many kilometers. As mentioned above, it is our contention that such a mass fire is composed of many hundreds or even thousands of individual fires of the type

described in the preceding sections. Such fires, provided they are distinct and separated physically from each other, can be characterized approximately by the sources (heat release rate and vorticity) that they would have separately. Under these circumstances the velocity field can be represented as follows:

$$\vec{u}(\vec{r}) = \sum_{k=1}^{K} (Q_k)^{1/5} \sum_{j=1}^{J} \vec{w} \left\{ (\vec{r} - \vec{r}_{jk})/(Q_k)^{2/5} \; ; \; \eta \right\} \qquad (37)$$

Here, $\vec{u}(\vec{r})$ is the composite velocity field induced by fires at nominal locations $\vec{r}_{jk}$ and of strength Q_k. The quantity $\vec{w}$ is the dimensionless flow field calculated above for a single fire. The dependence on ambient quantities is suppressed for clarity.

In practice, the precise locations and strengths of the individual fires cannot be predicted with any certainty. A more reasonable approach would be to regard these quantities as random variables, subject to certain overall constraints. The distribution function governing the strengths and locations of the fires could be based on the geometry and material composition of the burning area, together with the ignition and/or firespread scenario. Figure (8) shows an example of what can be done. A one kilometer square area is seeded with one hundred fires distributed uniformly in space. The fires are also distributed uniformly over five discrete strengths starting at 1.2×10^9W, with each successive size one half the previous value, for a total rate of heat release of approximately 4.7×10^{10}W. The shaded circles denote the actual burning areas assuming a combustible fuel density consistent with a heat release rate of $3 \times 10^5 \mathrm{W/m^2}$. This is well below that obtained from burning a variety of crude oil pool fires. Even so, the figure shows that less than fifteen percent of the area is actually burning.

The locations and strengths are obtained using a random number generator, and are subject only to the constraint that no two burning

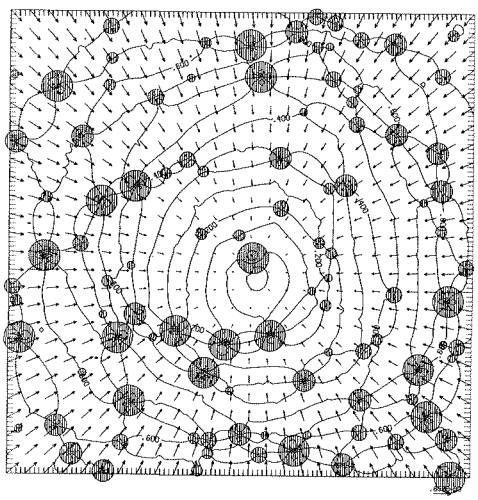

Figure 8. Ground level flow induced by 100 fires burning in one kilometer square. The total heat release is 4.7×10^{10}W and the peak velocity is 10m/s.

areas overlap. Note that the dimensionless velocity fields need only be calculated once for a given fractional radiative loss η. The values of the radial and vertical dimensionless velocity components are stored for each of the twenty thousand cells in which the numerical solutions are obtained. Similarity, the angular dependence of the asymptotic solutions are tabulated for one thousand values of the polar angle. The ground level velocity components for each of the one hundred fires are then computed on the 100 x 100 grid illustrated by the tick marks on the boundary using eq. (37). The velocity vectors at every fourth point are shown. Speed contours calculated from the full 100 x 100 grid are also displayed.

The peak values for the computed velocities are approximately ten meters per second. This may be compared with an experimental mass fire burn reported by Adams et.al.(27). The nominal burn area was .45 km on a side surrounded by a 300 M wide cleared area on each side. The peak convective heat release was 2 x 10^{10} W, with the brush fuel organized into thirty continuous rows. The average peak inflow velocity was 4.2 m/with 10m/s. total horizontal velocities at several locations reported. Given the numerous detailed differences between the calculated and experimental fire scenarios, the relatively good agreement between computed and measured velocities cannot be regarded as conclusive evidence for this approach. Still, the results are encouraging; particularly since no angular momentum induced firewhirl phenomena need be invoked to explain such relatively large ground level velocities.

For still larger fires, the burning area is divided into one kilometer squares. This represents a useful resolution scale for describing a large city or industrial area. The fires within each square are laid down as described above. Figure (9) shows the flow pattern induced by a 5 km x 1 km mass fire. The calculation of the contribution of each fire to the flow in its own square is performed as before. However, examination of eq. (37) shows that the contribution of the fires in remote squares can be greatly simplified. The inner sum (over j) for fires of a given size in a single square can be replaced by J times that of a single fire acting at the centroid of fires of strength Q_k for that square. Thus, the entire flow pattern (involving 500 fires) can be computed in about 30 seconds of computer time per square kilometer on a CDC Cyber 205 operating in scalar mode. This computing time is quite insensitive to the overall mass fire size, and is ideally suited for parallel computation.

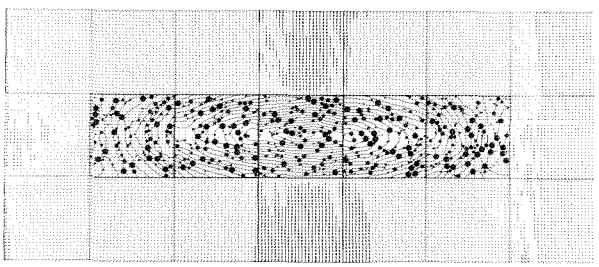

Figure 9. Ground level flow induced by 500 fires burning in 5 Km strip. The total heat release is 2.4×10^{11}W and the peak velocity is 50m/s.

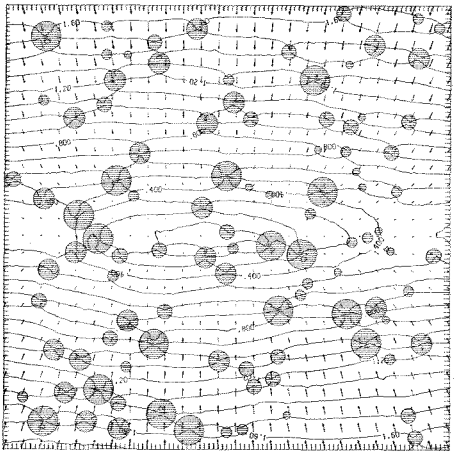

Figure 10. Detail showing central square of flow in Fig. 9.

A detail from this calculation, the center square kilometer of the burning region, is shown in Figure (10). Note that although the overall calculation encompasses an area of 7 Km x 3 Km, individual features with a length scale of less than ten meters (individual plume half widths) are preserved with no loss in accuracy. This highly granular structure of the mass fire model leads to predictions of nearly fifty meters per second in peak ground level velocity. This type of "subgrid model", which is based entirely on the theory and experiments described in earlier sections, is completely beyond the capability of purely numerical finite difference calculations. As an example, the computation illustrated in Figs. (9) and (10) would require 2-4 x 10^8 grid points to directly solve for the velocities at a resolution comparable to that displayed. (This scale computation is well beyond the capabilities of existing computers.) Moreover, the methods described here have been applied to scenarios involving many times the area and number of fires shown, without heroic efforts. Indeed, simulations involving tens of thousands of fires spread over hundreds of square kilometers are quite feasible with existing computers.

Concluding Remarks

A methodology for calculating the flows induced by fires has been presented. The approach requires a blend of analysis, experiment, and computation that emphasizes the strengths of each of these elements. Although the research was motivated by scenarios generated for the Nuclear Winter hypothesis, it offers a new approach for the analysis of both time averaged and fluctuating phenomena in fires, regardless of origin. We believe that the insights to be gained from this approach are not limited to fluid mechanics. The analysis of combustion processes in particular will require an economical description of the large eddy structure generated in fire plumes. The evolving experimental data base together with extensions of the kinematic analysis to time dependent flows will provide a challenging test of these ideas.

Acknowledgement

This research was supported in part by the Defense Nuclear Agency.

REFERENCES

1. Zukoski, E.E., "Fluid Dynamic Aspects of Room Fire", in Fire Safety Science, Proceedings of the First International Symposium, ed. C.E Grant and P.J. Pagni, pp. 1-23, Hemisphere, Washington, D.C. 1986.

2. Carrier, G.F., Fendell, F., and Feldman, P.S., Comb. and Sci. Tech., 4, p. 135, 1984.

3. Taylor, G.I., J. Aerospace Sciences 25, p. 464, 1958.

4. McCaffrey, B.J., Combustion and Flame 52, p. 149, 1983.

5. Committee on the Atmospheric Effects of Nuclear Explosions, "The Effects on the Atmosphere of a Major Nuclear Exchange", National Academy Press, Washington, D.C., 1985.

6. Carrier, G.F., Fendell, F., and Feldman, P.S., J. Heat Transfer, 107, p. 19, 1985.

7. Marcus, S., Krueger, S., Rosenblatt, M., "Numerical Simulation of Near-Surface Environments and Particulate Clouds Generated by Large-Area Fires", Defense Nuclear Agency Technical Report DNA-TR-87-1, Washington, D.C. 1987.

8. Small, R.D., Larson, D.A., Remetch, D., and Brode, H.L., "Analysis of the Burning Region and Plume of a Large Fire", Defense Nuclear Agency Technical Report DNA-TR-86-401, Washington, D.C. 1986.

9. Cotton, W.R., American Scientist, 73, p. 275, 1985.

10. Rehm, R.G., and Baum, H.R., J. Res. Nat. Bur. Stds, 83, p. 297, 1978.

11. Turner, J.S., Buoyancy Effects in Fluids, pp. 6-9, Cambridge University Press, Cambridge, 1973.

12. Boisvert, R.F., Howe, S.E., and Kahaner, D.K., "Guide to Available Mathematical Software", National Bureau of Standards Report NBSIR 84-2824, Washington, D.C. 1984.

13. Oberhettinger, F., "Hypergeometric Functions", in Handbook of Mathematical Functions with Formulas Graphs, and Mathematical Tables, ed. M. Abramowitz and I.A. Stegun, National Bureau of Standards Applied Mathematical Series 55, pp. 555-567, U.S. Govt. Printing Office, Washington, D.C. 1964.

14. Hasemi, Y. and Tokunaga, T., J. Heat Transfer, 108, p. 882, 1986.

15. Heskestad, G., Fire Safety Journal, 5, p. 109, 1983.

16. Cetegen, B., Zukoski, E.E., and Kubota, T., "Entrainment and Flame Geometry of Fire Plumes", National Bureau of Standards Report GCR 82-402, Washington, D.C. 1982.

17. Rockett, J., Sugawa, O., and McCaffrey, B., in preparation.

18. Hagglund, B. and Persson, L.E., "The Heat Radiation from Petroleum Fires", FOA Rapport C 20126-D6(A3), Stockholm, 1976.

19. McCaffrey, B.J., Some Measurements of the Radiative Power Output of Diffusion Flames", 1981 Western States Combustion Institute Meeting, Pullman, Paper WSS/CI 81-15, 1981.

20. Keltner, N., private communication, 1986.

21. McCaffrey, B.J., "Purely Buoyant Diffusion Flames", National Bureau of Standards Report NBSIR 79-1910, (1979).

22. Cox, G., and Chitty, R., Fire and Materials 6, p. 127, 1982.

23. Wechman, E.J., "The Structure of the Flowfield Near the Base of a Medium-Scale Pool Fire", Ph.D. Thesis, University of Waterloo, Waterloo, 1987.

24. Walker, N.L. and Moss, J.B., Comb. Sci. and Tech. 41, p. 43, 1984.

25. Fischer, S.J., Hardouin-Duparc, B., and Grosshandler, W.L., Combustion and Flame, 70, p. 291, 1987.

26. Schonbucher, A., Arnold, B., Balluff, C., Bieller, V., Barotz, W., Kasper, H., Kaufmann, M., and Schiess, N., "Simultaneous Observations of Organized Density Structures and the Visible Field in Pool Fires", Twenty-First International Symposium on Combustion, The Combustion Institute, Pittsburgh, in press.

27. Adams, J.S., Williams, D.W., and Tregellas-Williams, J., "Air Velocity, Temperature, and Radiant-Heat Measurements Within and Around a Large Free-Burning Fire", Fourteenth Symposium (Int'l) on Combustion, p. 1045, The Combustion Institute, Pittsburgh, 1973.

28. Yumoto, T., and Loseki, H. "Effect of Tank Diameter on Combustion Characteristics of Heptane Tank Fires", Report of Fire Research Institute of Japan 55 (in Japanese), 1983.

29. Gordon, W., and McMillan, R.D., Fire Technology 1, p. 52, 1965.

30. Byran, G.M., and Nelson,R.M., Fire Technology 6, p. 102, 1970.

31. Kung, H.S., and Starrianidis, P., "Buoyant Plumes of Large-Scale Pool Fires", Nineteenth Symposium (International) on Combustion, p. 905, The Combustion Institute, Pittsburgh, 1982.

32. Raj, P.K., "Analysis of JP-4 Fire Test Data and Development of a Simple Fire Model", ASME Paper 81-HT-17, 1981.

33. Anon, "Report of Oil Fire Experiment", Japan Society of Safety Engineering (Kerosene) (in Japanese), 1981.